Materials Science and Technology 38 (2022) 1291-1299

Critical assessment: the strength of undeformed pearlite

H. K. D. H. Bhadeshia† and A. R. Chintha*

†Queen Mary University of London
School of Engineering and Materials Science, London E1 4NS, U. K.

*Tata Steel Limited
Research and Development Division, Jamshedpur, India

Materials Science and Technology 38 (2022) https://doi.org/10.1080/02670836.2022.2079295

Abstract

The dependence of the proof strength of undeformed pearlite on its interlamellar spacing is examined in detail, with a view to resolving the plethora of relationships that exist in the research literature. It is found by the analysis of published data that the Hall-Petch equation is best suited to explain the strength, not simply on the basis of empirical fit, but even when examined in a Bayesian framework. Furthermore, it is the only relationship that gives a physically meaningful value to the friction stress. The reasons why previous analyses have failed to resolve this issue are examined and explained. It is discovered that ferrite in interstitial-free iron is, at an identical length scale, stronger in yield than the ferrite within pearlite.

1 Introduction

The strength $\sigma_{\rm y}$ of fully pearlitic steel that is in an initially undeformed state depends mostly on the interlamellar spacing $S_{\rm I}$. However, the exact form of the function $\sigma_{\rm y} = f\{S_{\rm I}\}$ has been the subject of debate for a number of reasons, the most common of which is related to the unphysical value of the strength when the interlamellar spacing is set to be infinite [e.g., 1]. Although the present work is limited to pearlite, the dilemma is generic. It often is suggested that a variety of relationships can adequately represent measured strength data assuming empirical fitting to a length parameter (e.g. [p. 230, 2],[3]). There even has been an effort to prove that all such relationships should really be described by a function that involves the relaxation of an epitaxially deposited film, whence the space available for dislocation sources to operate is the determining factor [4].

Pearlite, of course, is not a single phase, nor can it be described accurately as consisting of alternating plates of cementite and ferrite [5]. Nevertheless, yielding must first begin in the ferrite and therefore, the interlamellar spacing must be taken as the constraining feature to the transmission of yield through the structure as a whole. In this work, we examine whether $f\{S_{\rm I}\}$ is simply an empirical function or is it possible to distinguish between the

variety of models given the data. We begin by outlining the basis of some of the proposed mechanisms and then analysing a compilation of data.[1]

2 Hall-Petch relationships

Slip does not occur homogeneously in a polycrystalline material; some crystals will be better oriented than others for the resolved shear stress to initiate dislocation motion on the relevant slip system. Macroscopic yielding is defined as the propagation of plastic deformation between grains, indirectly by stress concentrations that accumulate at grain boundaries rather than by dislocations in one grain navigating their way into adjacent grains, a process that would require a large degree of crystallographic continuity.

Figure 1 illustrates the mechanism, whereby the crystal on the left happens to be favourably oriented with respect to the applied shear stress τ_a, leading to a pile-up of like-dislocations at the grain boundary. Assuming that the length of the slip plane is equal to the mean lineal intercept $\overline{L}$ that defines the grain size, the number of dislocations involved in the pile-up, at equilibrium with the stress, is given for large n by

$$n = \frac{\overline{L}\tau_\mathrm{a}}{2A} \qquad \text{with} \qquad A = E_\mathrm{s}|\mathbf{b}|\,[\sin^2\phi + (1-\nu)\cos^2\phi]/2\pi(1-\nu) \tag{1a}$$

where ϕ is the angle between the dislocation line and its Burgers vector $\mathbf{b}$, E_s is the shear modulus and ν is the Poisson's ratio [8, 9]. The pile-up has the effect of concentrating stress to an extent $n\tau_\mathrm{a}$ at the tip of the pile-up so substituting for n using Equation 1a gives the stress there as

$$\tau_\mathrm{tip} = n\tau_\mathrm{a} = \frac{\overline{L}\tau_\mathrm{a}^2}{2A} \qquad \text{so that} \qquad \tau_\mathrm{a} = \sqrt{\frac{\tau_\mathrm{tip}2A}{\overline{L}}}. \tag{1b}$$

If it is assumed that plastic deformation propagates when τ_tip reaches a constant critical value τ_c and after accounting for the friction stress τ^f which must also be overcome, the form of the classical Hall-Petch equation [10–12] is recovered:

$$\tau_\mathrm{y} = \sqrt{\tau_\mathrm{c}2A} \times (\overline{L})^{-\frac{1}{2}} + \tau^\mathrm{f} \tag{1c}$$

where τ_a has been replaced by the shear yield strength τ_y. If, in a polycrystalline material, the shear and uniaxial tensile stresses are related by the Taylor factor M [13], then it follows that

$$\sigma_\mathrm{y} = \underbrace{M\sqrt{\tau_\mathrm{c}2A}}_{k_\mathrm{HP}} \times (\overline{L})^{-\frac{1}{2}} + \sigma^\mathrm{f} \tag{1d}$$

where k_HP is the Hall-Petch coefficient. Dislocation pile-ups of the kind illustrated in Figure 1 are often not observed experimentally; instead, arrangements of dislocations described as *forests* within grain interiors are more common in iron. The general form of Equation 1d is nevertheless maintained when the forest-dislocations are under stress from grain boundary steps [14, 15]. This is because the density ρ_f of such dislocations is proportional to the grain boundary area per unit volume, i.e., $2/\overline{L}$ and since the flow stress depends on $\sqrt{\rho_\mathrm{f}}$, the net outcome remains the inverse square root dependence of flow stress on grain size.

[1] It is assumed throughout that the dislocation density of undeformed pearlite does not depend on the interlamellar spacing. Data from [6, 7] indicate dislocation densities of $0.7 \times 10^{14}\,\mathrm{m}^{-2}$ and $1.1 \times 10^{14}\,\mathrm{m}^{-2}$ for S_I equal to 0.09 and 0.13 µm, respectively; these densities are well within typical errors associated with such measurements.

Irrespective of the detailed mechanism, we note that σ^{f} is well defined.

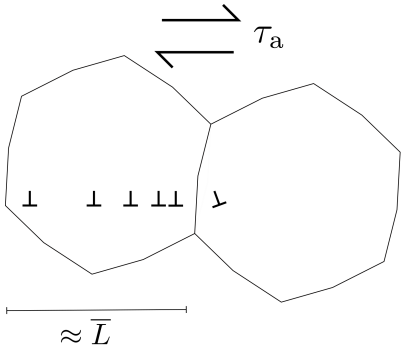

Figure 1: How the stress concentration due to a pile-up of dislocations due to a single-ended source on a slip plane in the crystal on the left activates a dislocation source in an adjacent grain, thereby implementing general yielding in a polycrystalline material.

2.1 Langford model for yield of pearlite

Langford's interest in the severe deformation associated with the drawing of both ferritic and pearlitic wires led him to develop a model for plastic deformation that incorporates dislocation mechanisms on a scale that respects the fine structure of pearlite. The increment of shear strain (γ) caused by the translation of a dislocation of Burgers vector $\mathbf{b}_\theta$ across a cementite (θ) plate of length L_1, assuming that the vector makes an angle of 45° with L_1, is [16]

$$\Delta\gamma = \frac{|\mathbf{b}_\theta|}{\sqrt{2}L_1} \tag{2a}$$

and the work necessary to achieve this is the product of the shear stress and plastic shear-strain, which consists of components due to the the friction shear stress and the line energy Γ_θ of the dislocation, assuming that the latter has to be created:

$$\tau_\theta \Delta\gamma = \tau_\theta^{\mathrm{f}} \Delta\gamma + \frac{\Gamma_\theta L_2}{L_1 L_2 L_\theta} \tag{2b}$$

where L_i are the dimensions of the cementite plate, noting that for pearlitic cementite, the thickness $L_\theta \ll L_1$ or L_2. It follows by combining these equations that

$$\tau_\theta = \tau_\theta^{\mathrm{f}} + \sqrt{2}\frac{\Gamma_\theta}{|\mathbf{b}_\theta| L_\theta}. \tag{2c}$$

The ambient temperature Vickers hardness of almost pure cementite in cast iron is found to be just over 1000 HV corresponding to an ultimate strength in tension of about 3.3 GPa (hardness/3, [17]). Assuming that the friction stress in tension is smaller than this by about 10%, the *shear* friction strength $\tau_\theta^{\mathrm{f}} \approx 1.5$ GPa.

Cementite has a primitive lattice with space group *Pnma* and given its large lattice parameters, the magnitude of any Burgers vector of a slip dislocation will inevitably be large. Since the most commonly observed slip system is (010)[001] [18, 19], $|\mathbf{b}_\theta| = 0.45165$ nm, which is much larger than that of any slip dislocation in austenite or ferrite.

The energy per unit length of a dislocation in an average population of screw and edge

characters is given by [20]

$$\Gamma_\theta \approx \frac{E_s^\theta |\mathbf{b}_\theta|^2}{4\pi} \frac{1-0.5\nu_\theta}{1-\nu_\theta} \ln\left\{\frac{L_\infty}{|\mathbf{b}_\theta|}\right\} + \Gamma_\theta^* \tag{2d}$$

where Γ_θ^* is the core energy per unit length; in the absence of information, this is taken here to be identical to that in ferrite, i.e., $\Gamma_\theta^* \approx 3 \times 10^{-10}\,\mathrm{J\,m^{-1}}$ [21]. The extent of the elastic-strain field L_∞ of the dislocation depends on stress screening by other dislocations; assuming that there are more dislocations present in the adjacent ferrite (α), this length could be approximated as the interlamellar spacing, typically a micrometre. The isotropic shear modulus and Poisson's ratio for cementite have been estimated using first principles calculations and averaging to be 75 GPa and 0.35 respectively [22, 23]. Using these values, $\Gamma_\theta \approx 1.2 \times 10^{-8}\,\mathrm{J\,m^{-1}}$. With these data and assuming that the cementite thickness $L_\theta = 0.2\,\mu\mathrm{m}$ and the value of the friction stress becomes $\tau_\theta \approx 1.7\,\mathrm{GPa}$.[2]

The shear yield strength of pearlite was then expressed using the Hall-Petch relation:[3]

$$\tau_\mathrm{P} = \tau_\alpha^\mathrm{f} + \sqrt{2E_s^\alpha |\mathbf{b}_\alpha| \tau_\theta \frac{2-\nu_\alpha}{4\pi(1-\nu_\alpha)}} \left(\frac{1}{L_\alpha}\right)^{\frac{1}{2}} \tag{2e}$$

where L_α is the thickness of ferrite, which under equilibrium conditions is related to the cementite thickness L_θ by the equilibrium fraction of cementite in a eutectoid steel. The term containing the Poisson's ratio is determined by an assumption of a mixed population of screw and edge dislocations orientations. Langford's model never seems to have been tested against data but Equation 2e leads to a gross overestimation of the yield strength of pearlite, even when τ_θ is reduced from the estimated 1.7 GPa to 0.2 GPa. For example, with $L_\theta = 0.02\,\mu\mathrm{m}$, $L_\alpha = 0.118\,\mu\mathrm{m}$ (giving $S_\mathrm{I} = 0.138\,\mu\mathrm{m}$), $\tau_\alpha^\mathrm{f} = 77/2\,\mathrm{MPa}$, $\tau_\theta^\mathrm{f} = 1700\,\mathrm{MPa}$, $\mathbf{b}_\theta = 0.452\,\mathrm{nm}$, $|\mathbf{b}_\alpha| = 0.25\,\mathrm{nm}$, the shear stress given by Equation 2e comes to $\tau_\mathrm{P} = 2.5\,\mathrm{GPa}$, i.e., a tensile strength twice that value whereas the actual tensile strength for that interlamellar spacing is 580 MPa. Reducing τ_θ^f to 200 MPa makes $\tau_\mathrm{P} = 1.8\,\mathrm{GPa}$.

It is known from direct observations using transmission electron microscopy that the yield strength of pearlite is that needed to move dislocations in ferrite between "impenetrable" cementite walls; both yielding and work hardening are said to be controlled by dislocation activity within the ferrite [1]. Therefore, the assumption in the Langford model that a pile-up in ferrite will induce flow in the adjacent cementite, is not justified given the tremendous disparity in the strengths of the two phases. Until the stress within the ferrite accumulates to a sufficient level, the cementite must remain elastically strained or strained to fracture.

However, bearing in mind that a pearlite colony is an interpenetrating bicrystal of α and θ [5], initial yielding may be determined by dislocation pile-ups at the α/θ interfaces stimulating other adjacent ferrite to yield, in which case a Hall-Petch relation would prevail with the cementite acting simply as a means to transmit stress. Given that the stress ahead of a dislocation pile-up diminishes with distance beyond its tip, there is a special strengthening effect because this intervening cementite makes it more difficult for yielding to be stimulated

[2] The magnitude of this stress contradicts the statement in the original work [16] that Equation 2c leads to a flow stress of cementite that is less than that of pearlite. It is possible that Langford neglected to consider τ_θ^f since its value was not stated.

[3] The ratio $|\mathbf{b}_\theta|/|\mathbf{b}_\alpha|$ in the original treatment is removed from this equation because it does not seem justified. Langford also assumed that the cementite deformation occurs by the propagation of a partial dislocation, which also is not justified so the Burgers vector corresponding to the common slip system, i.e., [001] is substituted. Similarly, Langford's $2L_\alpha$ term has also been replaced by just L_α.

in the ferrite on the other side of the dislocation pile-up. This is separate from the usual strengthening due to the density of α/θ interfaces.

3 Analysis

Here we compare the yield strength against a variety of functions of the interlamellar spacing, with the data all associated with fully pearlitic steels containing similar concentrations of manganese and silicon, Figure 2.

The yield strength is seen to correlate somewhat better with $S_{\mathrm{I}}^{-\frac{1}{2}}$ than S_{I}^{-1}; furthermore, the intercept for the latter function, representing the friction stress is too large at 397 MPa when compared against the strength of single-phase ferrite. The inverse square-root dependence has previously been criticised as leading to a negative friction-stress at infinite interlamellar spacing [e.g., 1]; however, this is a consequence of analyses depending on limited data based on individual studies, a classic problem widely recognised in machine learning, of *overfitting* [24, 25]; such relationships then do not generalise well on independent experiments as is easily evident. This is illustrated in Figure 2a where data from individual experiments are plotted separately to reveal the large differences in slopes and intercepts when each plot covers a limited range of interlamellar spacing. Although the individual plots may exhibit high levels of correlation, they clearly would not generalise well on data from other experiments as is obvious by extrapolating any one of the straight lines.

Figure 2b shows an analysis based on the entire dataset, giving that $\sigma^{\mathrm{f}} = 128\,\mathrm{MPa}$ for the Hall-Petch $S_{\mathrm{I}}^{-\frac{1}{2}}$ dependence. Iron containing 500 ppm of carbon has $\sigma^{\mathrm{f}} = 100\,\mathrm{MPa}$ [26, 27]; this concentration agrees with an atom probe determination of the carbon concentration of ferrite within pearlite [28]. Pearlitic steels typically contain 0.3Si and 0.4Mn wt%, which using Leslie's solution strengthening data [29] gives a combined contribution of 33 MPa so that σ^{f} estimated in this way is 133 MPa, eminently consistent with the plot in Figure 2b represented by

$$\sigma_{\mathrm{y}} \approx 174 S_{\mathrm{I}}^{-\frac{1}{2}} + 128 \quad \mathrm{MPa} \tag{3}$$

with S_{I} in micrometres. It has to be concluded that one of the mistakes in fitting the Hall-Petch equation to limited data is to assume that σ^{f} can take on any value determined by best fit, whereas it is in fact easy to estimate its value independently. In regression analyses, the friction stress should take on a fixed value based on independent strength data, with the slope being the fitting parameter.

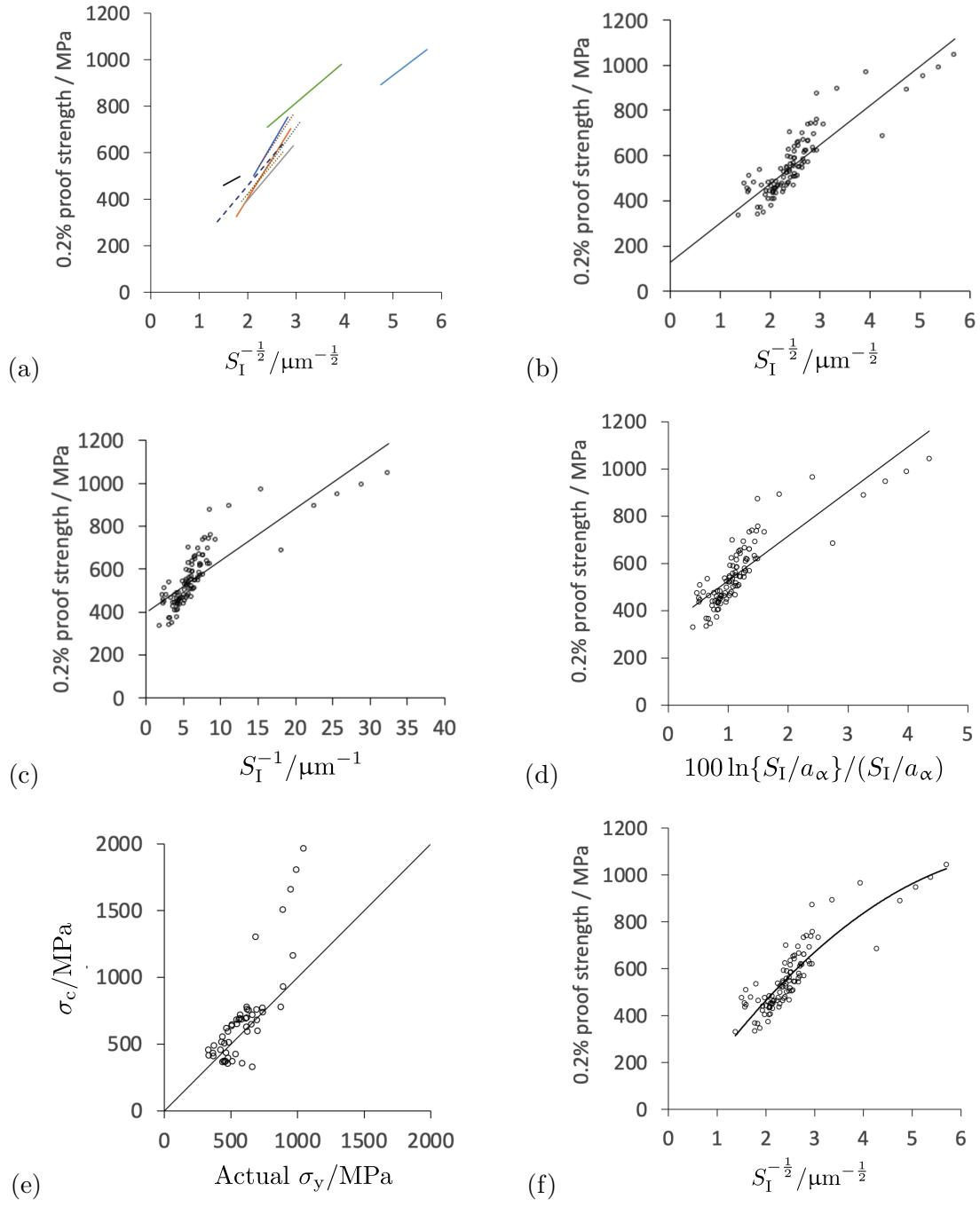

Figure 2: Yield strength of fully pearlitic, eutectoid, hypereutectoid and hypoeutectoid steels, none of which were in a plastically-deformed state prior to testing. (a) Hall-Petch best fits to individual datasets. (b) Plotted against the inverse of the square root of the interlamellar spacing, with a correlation coefficient of 0.87. The intercept on the vertical axis for an infinite spacing, corresponding to the friction stress in the Hall-Petch equation, is $\sigma^f = 128\,\text{MPa}$ with the slope of the regression line being $174\,\text{MPa}\,\mu\text{m}^{\frac{1}{2}}$. (c) Plotted against the inverse of the interlamellar spacing, with a correlation coefficient of 0.83. The intercept in this case is $\sigma^f = 397\,\text{MPa}$ and the slope, $24\,\text{MPa}\,\mu\text{m}^{\frac{1}{2}}$. (d) Correlation of strength against a more complex function originating in thin-film theory; the units of both S_I and the lattice parameter of ferrite are in μm, correlation coefficient 0.85. Data used in (b-d) from [1, 30–40]. (e) Proof strength calculated using Equation 5 against measured data [1, 30–32, 34–36, 38, 40]. The line has a unit slope and zero intercept. (f) Polynomial fit discussed later in the text.

It is instructive to compare the Hall-Petch coefficient k_{HP} from Equation 3 against data from interstitial-free ferrite, where the grain size of the recrystallised ferrite is comparable to the interlamellar spacing of pearlite. In Figure 3 the line fitted to the ferrite data [41] had the intercept fixed at $\sigma^{\mathrm{f}} = 50\,\mathrm{MPa}$ to be consistent with the value reported by Takaki [27] and can be represented by the equation:

$$\sigma_{\mathrm{y}} \approx 413(\overline{L})^{-\frac{1}{2}} + 50 \quad \mathrm{MPa} \tag{4}$$

where $\overline{L}$ is the grain size defined by the mean lineal intercept in units of μm. The interesting result is that the ferrite grains are stronger than the ferrite which yields within pearlite, at the same length scale. It is noted, however, that the smallest of grains in the interstitial-free steel were reported [41] to contain dislocation structures and were not isotropic in shape, which may contribute to some additional strength to the intersitial-free steel. The sensitivity of the ferrite grains to grain size is much greater (larger k_{HP}) than is the case for pearlite as a function of the interlamellar spacing. There are two reasons for this observation – first, that in a mixture of a soft and hard phase, the soft phase naturally yields first, but at a stress that is less than its yield strength in isolation [42, 43]. Secondly, fully pearlitic steels yield continuously because the interfaces between ferrite and cementite have a modicum of coherency, which means that they emit dislocations under stress [44]. The continuous yielding persists even when the structure is subjected to low-temperature heat-treatment of the kind associated with strain-ageing experiments. However, when the structure severely annealed to induce a loss of coherency, discontinuous yielding and Lüders strains follow. This kind of a partly coherent interface that emits dislocations under applied stress would reduce the proof strength whereas the grain boundaries between the recrystallised-ferrite crystals in the interstitial-free steel produced using accumulative roll bonding (as in [41]) are incoherent, large misorientation boundaries [45].

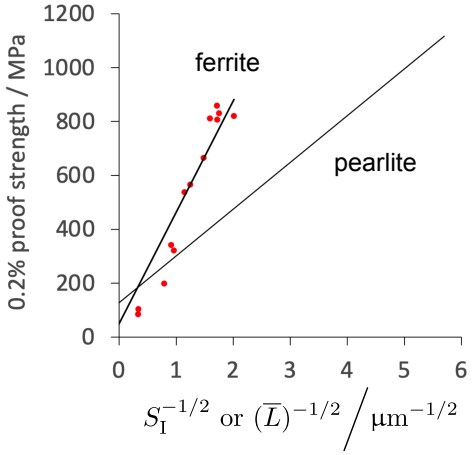

Figure 3: The ferrite data are from Tsuji et al. [41], representing interstitial free iron, and the line for pearlite is that from Figure 2b. The interstitial-free alloy has sufficient titanium to justify the assumption that the ferrite truly has a negligible carbon concentration in solution.

It is emphasised that there is no theoretical justification for $\sigma_{\mathrm{y}} \propto S_{\mathrm{I}}^{-1}$ relationship.[4] A calculation of the *lower-bound* value of the critical stress necessary to push a dislocation in ferrite between two non-deforming cementite particles of planar separation L_α, leads to the

[4] A composite model [15] in which cubic grains of size L_{soft} are surrounded by a hard phase of thickness L_{hard} predicts the strength to be a function of $L_{\mathrm{hard}}/L_{\mathrm{soft}}$ provided $L_{\mathrm{hard}} \ll L_{\mathrm{soft}}$, i.e., an inverse dependence on the size of the soft phase. However, with the ratio for pearlite is fixed by its chemical composition so the dependence of strength on interlamellar spacing vanishes in this scenario.

relationship [46, 47]

$$\sigma_{\rm c} = \sigma^{\rm f} + \frac{ME_{\rm s}|\mathbf{b}_\alpha|}{2\pi L_\alpha}\left(\frac{1-0.5\nu_\alpha}{1-\nu_\alpha}\right)\ln\left\{\frac{L_\alpha}{|\mathbf{b}_\alpha|}\right\} \tag{5}$$

where the term $L_\alpha = S_{\rm I}V_{\rm V}^\alpha$ is the thickness of the ferrite layer; $V_{\rm V}^\alpha$ is the volume fraction of ferrite. With $\sigma^{\rm f}$ given by Equation 3, the Taylor factor $M = 2.8$, $\nu_\alpha = 0.29$, Figure 2e shows that a reasonable correlation is obtained between the calculated and measured proof strengths; however, for data where $S_{\rm I} < 50\,{\rm nm}$, the strength is grossly overestimated. It is important to note that L_α is not proportional to $S_{\rm I}$ because the proportion of ferrite in pearlite depends on its carbon concentration – fully pearlitic microstructures are generated in hypoeutectoid or hypereutectoid steels by suppressing the transformation temperature into the Hultgren extrapolation region [e.g., Figure 12.7, 48]; such data are included in the present work.

An approach somewhat analogous to that of Langford has been claimed to pose a fundamental challenge to the Hall-Petch relationship. It has its origin in the semiconductor scenario, with an equation derived to estimate the elastic misfit strain that can be supported by a thin epitaxial layer deposited on a substrate of a different material. Beyond a critical thickness for a given misfit, the deposited layer should relax by the introduction of dislocations. With the assumption that a distance that is a multiple of this critical thickness must be used to account for the operation of dislocation sources, the strength is supposed to vary with grain size (here taken to be the interlamellar spacing) as [4]

$$\sigma_{\rm y} \propto \frac{\ln\{S_{\rm I}/a_\alpha\}}{S_{\rm I}/a_\alpha} \tag{6}$$

where a_α is the lattice parameter of ferrite to make the grain size dimensionless. Although the original paper [4] uses grain size and dimensionless grain size interchangeably in describing the relationship with strength, this procedure in fact introduces two dependencies on interlamellar spacing because

$$\frac{\ln\{S_{\rm I}/a_\alpha\}}{S_{\rm I}/a_\alpha} \equiv a_\alpha\left(\frac{\ln\{S_{\rm I}\}}{S_{\rm I}} - \frac{\ln\{a_\alpha\}}{S_{\rm I}}\right). \tag{7}$$

It isn't surprising, therefore, that the correlation of the data using the spacing term in Equation 6 is almost identical to that against $S_{\rm I}^{-1}$, *cf.* Figures 2c,d because the inverse dependence is dominant in Equation 7 for $S_{\rm I} \gtrsim 0.2\,\mu{\rm m}$, which represents data for the majority of fully pearlitic steels, with small differences between these two relationships evident for the finest of spacings.

The proportionality constant in Equation 6 when converted into a dimensionless number by dividing with the Young's modulus (E) is expected to be of the order of unity [4]. The fitted line in Figure 2d can be written as:

$$\sigma_{\rm y} = 188.9\left(\frac{100\ln\{S_{\rm I}/a_\alpha\}}{S_{\rm I}/a_\alpha}\right) + 339 \quad {\rm MPa} \tag{8}$$

$$\text{so that } \frac{\sigma_{\rm y}}{E} = \underbrace{\frac{1.889\times10^4}{E}}_{\text{coefficient}}\left(\frac{\ln\{S_{\rm I}/a_\alpha\}}{S_{\rm I}/a_\alpha}\right) + \frac{339}{E}. \tag{9}$$

Since $E = 2.1\times10^5\,{\rm MPa}$, the coefficient has a dimensionless value 0.09, which is about a

tenth of that expected from Equation 1.3 of [4]. It follows that if the coefficient is close to unity then the theory should greatly overestimate the strength.

Notice that for the reason explained earlier, the form of the term $\ln\{S_\mathrm{I}/a_\alpha\}/(S_\mathrm{I}/a_\alpha)$ in Equation 7 is not similar to that of $\ln\{L_\alpha/|\mathbf{b}_\alpha|\}/(L_\alpha/|\mathbf{b}_\alpha|)$ of Equation 5.

Equation 3 works rather well on independent data; Figure 4 illustrates careful measurements made on simple, model eutectoid-alloys: Fe-0.78C, Fe-0.8C-0.99Si, Fe-0.82C-0.97Mn, Fe-0.82C-2.01Si, Fe-0.77C-1.96Mn, Fe-0.79C-1Si-1Mn wt% [49]. Some of these alloys contain up to 2 wt% of substitutional solutes, and yet agreement is good even though σ_f is unchanged from the value in Equation 3. This is because the strength due to interlamellar spacing represent the largest proportion of total strength, more so at the smallest of interlamellar spacings. Therefore, the error due to the neglect of solid solution effects will be reflected in the noise, i.e., the scatter about the expectation. Solid-solution effects are in fact difficult to account for given that only average concentrations are available, whereas there is some partitioning expected between the ferrite and cementite at all transformation temperatures [50].

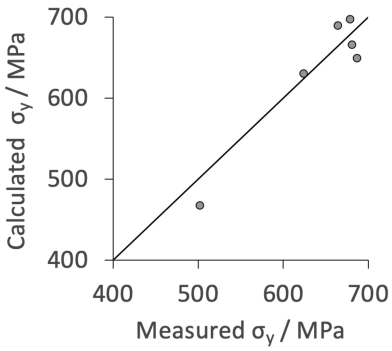

Figure 4: Comparison of the yield strength of pearlite as calculated using Equation 3 against experimental data due to Fu et al. [49]. The line has unit slope and zero intercept.

It is tempting when looking at the plots in Figure 2 to suggest that trend for relatively coarse interlamellar spacings is different to that at the finest of spacings. In other words, that the strength is a non-linear function of S_I. Figure 2f shows a polynomial fit (order 2) where the slope becomes more gentle at large spacings. However, the correlation coefficient at 0.88 is almost identical to that for the ordinary Hall-Petch linear fit at 0.87. Furthermore, there is no theoretical backing to such a relationship.

3.1 Analysis in Bayesian framework

The regression analysis of strength data results in unique values of the best fit weights, which in the case of linear analysis represent the slope and intercept, without commenting on how these values depend, for example, on the size of the dataset. On the other hand, in a Bayesian framework, each weight has a *distribution* of possible values, reflecting the level of certainty about the weights given the dataset. The output is then not estimated as a single value but as a probability distribution. A greater certainty in the prediction corresponds to a narrow distribution of weights given the data. This is powerful because the method permits the uncertainty of any prediction to be quantified. This uncertainty is separate from the constant value of the perceived noise, σ_ν, in the output; the Bayesian uncertainty will vary with the location of the calculation in the input domain. Noise in this context

refers to repeated experiments giving different outcomes because of missing variables in the design of experiments or experimental error. The general principles have been described by MacKay [51–53].

To ensure that an empirical fit to data does not model noise (i.e., the overfitting problem), the data can be divided at random into a training and a test set, where the former is used to create the model and the latter to assess how it generalises on unseen experiments. Figure 5 shows two kinds of plots for fully pearlitic steels. It is evident that the Hall-Petch relationship is best suited to represent the propagation of yield across the structure of pearlite over a broad range of variation, with an an optimum fit to both the training and test data. In contrast, the other two functions only show consistency between experiment and calculations over a narrow range of strength, with the consequence that there are very many outliers.

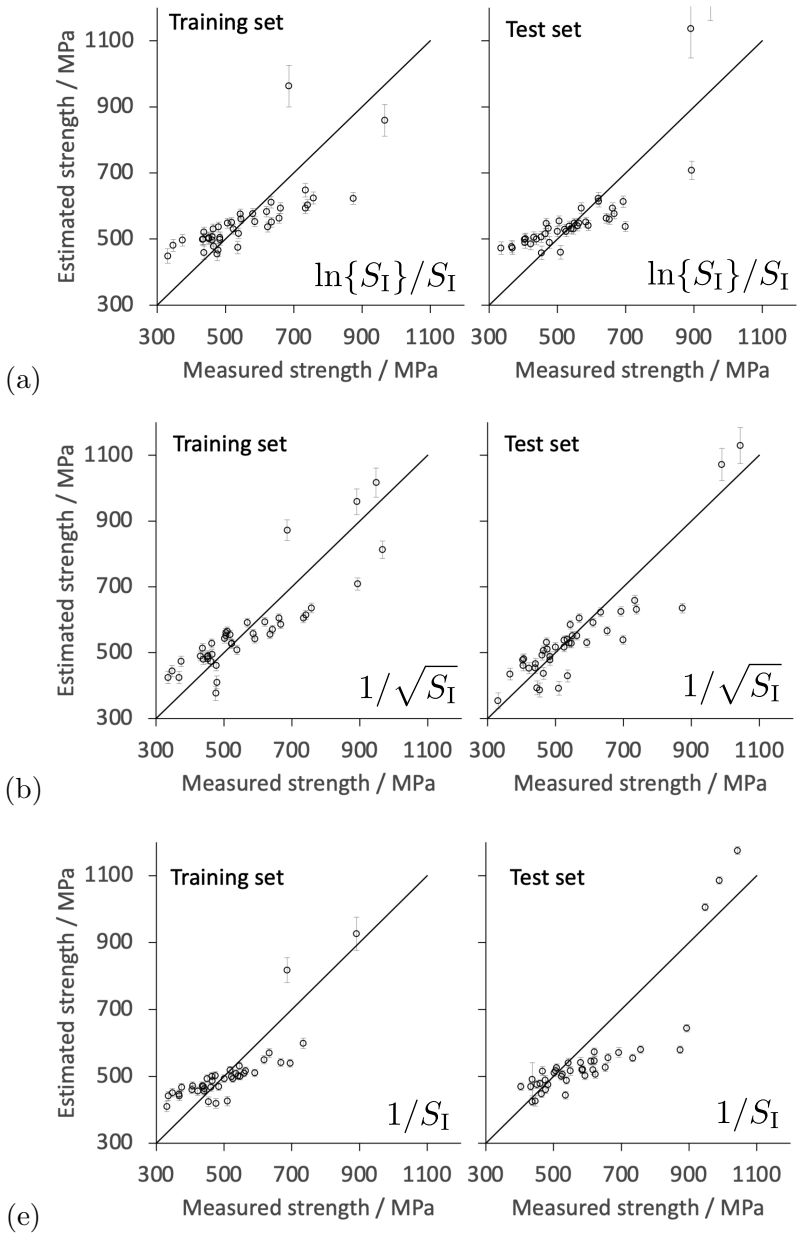

Figure 5: Linear regression in a Bayesian framework using the training data for model creation and the unseen test data to assess generalisation, using the method by MacKay [51, 52]. The uncertainty illustrated is due to the distribution of weights; the noise σ_ν has not been included in the error bars, for reasons of clarity. (a) Assuming that the strength varies with $\ln\{S_\mathrm{I}\}/S_\mathrm{I}$ (units µm), with $\sigma_\nu = \pm 0.13$. (b) The Hall-Petch relation, with $\sigma_\nu = \pm 0.11$. (c) The inverse relation, with $\sigma_\nu = \pm 0.11$.

The same method can be applied to include all three functions in a multiple linear regression within the Bayesian framework. Figure 6a shows an interesting consequence of the fact that the S_I^{-1} and $\ln\{S_\mathrm{I}\}/S_\mathrm{I}$ represent only a narrow range of strength; the error bars become very large outside of this range because these two functions deviate so much from measured data. On the other hand, the Hall-Petch relation nicely follows the general trend of the multiple regression function.

Figure 6b shows the significance in the multiple regression analysis, of each of the three

inputs $S_{\rm I}^{-1}$, $S_{\rm I}^{-1/2}$ and $\ln\{S_{\rm I}\}/S_{\rm I}$. The term $\sigma_{\rm w}$ represents the values of the regularisation constants, expressed as standard deviations of the implicit gaussians [51, 52]; in simple terms, it is related to the effectiveness of a particular input in explaining the variation in the output. The Hall-Petch parameter is again perceived to be the best at representing the variation of the strength of pearlite as a function of the interlamellar spacing.

It is noted that Occam's razor [54] is in the present case less useful as a method for distinguishing between the models because they all are linear functions with just the slope and intercept as coefficients.

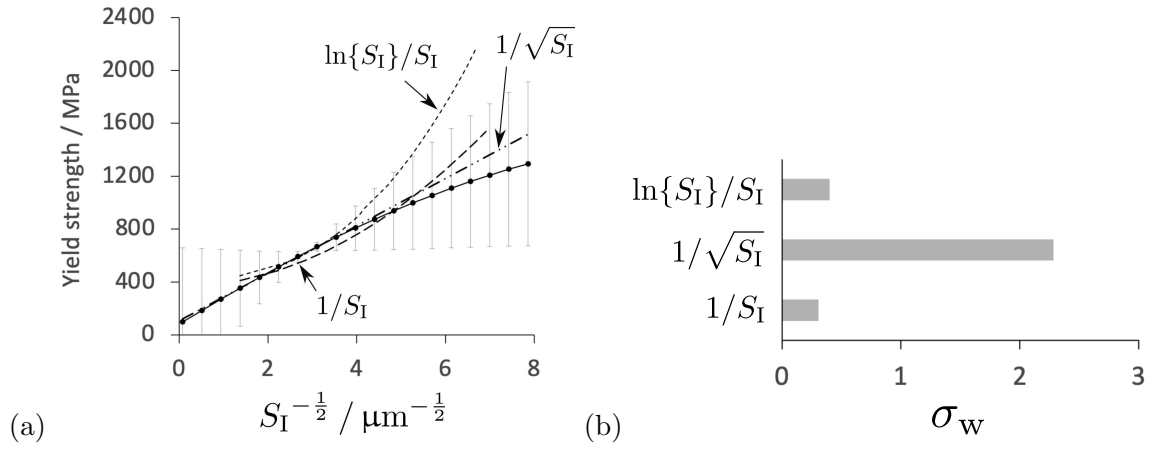

Figure 6: (a) The curve that includes uncertainties associated with the distribution of weights represents multiple linear regression, within an Bayesian framework, of predicted strength as a function of $S_{\rm I}^{-1}$, $S_{\rm I}^{-1/2}$ and $\ln\{S_{\rm I}\}/S_{\rm I}$. The perceived noise, not included in the plot, is $\sigma_\nu = \pm 0.09$. The other three curves are predictions using the individual models illustrated in Figure 5a-c. (b) The model perceived significance of each of the functions included in the multiple regression.

4 Conclusions

The Hall-Petch equation is found to be the most plausible representation of the proof strength of fully pearlitic steels, assuming that deformation begins in the much softer ferrite. The friction stress deduced with this equation is physically reasonable whereas that is not the case when other relationships are considered. Some of the problems perceived with the Hall-Petch equation in previous work are believed to be associated with overfitting the data and/or the use of limited data. A discovery is that ferrite in interstitial-free iron is, at the same length scale, stronger in yield than the ferrite within pearlite; its sensitivity to grain size is also much greater than that of pearlite to interlamellar spacing. The data compiled for the present work can be accessed so any future measurements can be added in order to avoid the overfitting problem described in the text:

https://www.phase-trans.msm.cam.ac.uk/2022/HP.xlsx

and the origins of the data are listed in the text. In all cases, irrespective of model, the perceived noise in the data is of the order ± 0.1, i.e., 10%, which might represent reasonable errors of measurement.

5 Acknowledgments

We are grateful to Professor David Dunstan for valued comments on a draft of this paper.

References

1. M. Dollar, I. M. Bernstein, and A. W. Thompson: 'Influence of deformation substructure on flow and fracture of fully pearlitic steel', *Acta Metallurgica*, 1988, **36**, 311–320.

2. R. E. Reed-Hill: Physical Metallurgy Principles: 2nd ed., Boston, USA: PWS Publishers, 1973.

3. E. M. Taleff, J. J. Lewandowski, and B. Pouladian: 'Microstructure-property relationships in pearlitic eutectoid and hypereutectoid carbon steels', *Journal of Metals*, 2002, **54**, 25–30.

4. Y. Li, A. J. Bushby, and D. J. Dunstan: 'The Hall-Petch effect as a manifestation of the general size effect', *Proceedings of the Royal Society A*, 2016, **472**, 20150890.

5. M. Hillert: 'The formation of pearlite', In: V. F. Zackay, and H. I. Aaronson, eds. *Decomposition of Austenite by Diffusional Processes*. New York, USA: Interscience, 1962:197–237.

6. X. Zhang, A. Godfrey, X. Huang, N. Hansen, and Q. Liu: 'Microstructure and strengthening mechanisms in cold-drawn pearlitic steel wire', *Acta Materialia*, 2011, **59**, 3422–3430.

7. N. Guo, T. Liu, B. Luan, B. Wang, and Q. Liu: 'Dislocation density and configuration in fully pearlitic steel during wire drawing', *Materials Research Innovations*, 2014, **18**, S4:249–254.

8. J. D. Eshelby, F. C. Frank, and F. R. N. Nabarro: 'XLI. The equilibrium of linear arrays of dislocations.', *The London, Edinburgh, and Dublin Philosophical Magazine and Journal of Science*, 1951, **42**, 351–364.

9. J. C. M. Li, and Y. T. Chou: 'The role of dislocations in the flow stress grain size relationships', *Metallurgical Transactions*, 1970, **1**, 1145–1159.

10. E. O. Hall: 'The deformation and ageing of mild steel: III discussion of results.', *Proceedings of the Physical Society B*, 1951, **64**, 747–753.

11. N. J. Petch: 'The cleavage strength of polycrystals', *Journal of the Iron and Steel Institute*, 1953, **174**, 25–28.

12. E. O. Hall: Yield point phenomena in metals and alloys: New York, USA: Plenum Press, 1970.

13. G. I. Taylor: 'Plastic strain in metals', *Journal of the Institute of Metals*, 1938, **62**, 307–324.

14. J. C. M. Li: 'Petch relation and grain boundary sources', *Transactions of the Metallurgical Society of the AIME*, 1963, **227**, 239–247.

15. M. Kato: 'Hall-Petch relationship and dislocation model for deformation of ultrafine-grained and nanocrystalline metals', *Materials Transactions, JIM*, 2014, **55**, 19–24.

16. G. Langford: 'Deformation of pearlite', *Metallurgical Transactions A*, 1977, **8**, 861 – 875.

17. D. Tabor: 'The hardness and strength of metals', *Journal of the Institute of Metals*, 1951, **79**, 1–12.

18. A. Inoue, T. Ogura, and T. Muramatsu: 'Burgers vectors of dislocations in cementite crystal', *Scripta Metallurgica*, 1977, **11**, 1–5.

19. J. Alkorta, and J. G. Sevillano: 'Assessment of elastic anisotropy and incipient plasticity in fe3c by nanoindentation', *Journal of Materials Research*, 2012, **27**, 45–52.

20. N. Hansen, and D. Kuhlmann-Wilsdorf: 'Low energy dislocation structures due to unidirectional deformation at low temperatures', *Materials Science & Engineering*, 1986, **81**, 141–161.

21. E. Clouet, L. Ventelon, and F. Wilaime: 'Dislocation core energies and core fields from first principles', *Physical Review Letters*, 2009, **102**, 055502.

22. C. Jiang, S. G. Srinivasan, A. Caro, and S. A. Maoly: 'Structural, elastic, and electronic properties of Fe_3C from first principles', *Journal of Applied Physics*, 2008, **103**, 043502.

23. H. K. D. H. Bhadeshia: 'Cementite', *International Materials Reviews*, 2020, **65**, 1–27.

24. H. K. D. H. Bhadeshia: 'Neural networks in materials science', *ISIJ International*, 1999, **39**, 966–979.

25. H. Pous-Romero, I. Lonardelli, D. Cogswell, and H. K. D. H. Bhadeshia: 'Austenite grain growth in a nuclear pressure vessel steel', *Materials Science & Engineering A*, 2013, **567**, 72–79.

26. S. Takaki, K. Kawasaki, and Y. Kimura: 'Mechanical properties of ultra fine grained steels', *Journal of Materials Processing Technology*, 2001, **117**, 359–363.

27. S. Takaki: 'Influence of alloying elements on the Hall-Petch coefficient in ferritic steel', *Materials Science Forum*, 2012, **706-709**, 181–185.

28. N. Maruyama, T. Tarui, and H. Tashiro: 'Atom probe study on the ductility of drawn pearlitic steels', *Scripta Materialia*, 2002, **46**, 599–603.

29. W. C. Leslie: 'Iron and its dilute substitutional solid solutions', *Metallurgical Transactions A*, 1972, **3**, 5–23.

30. T. Gladman, I. D. McIvor, and F. B. Pickering: 'Some aspects of the structure-property relationships in high-C ferrite-pearlite steels', *Journal of the Iron and Steel Institute*, 1972, **210**, 916–930.

31. J. M. Hyzak, and I. M. Bernstein: 'The role of microstructure on the strength and toughness of fully pearlitic steels', *Metallurgical Transactions A*, 1976, **7**, 1217–1221.

32. J. P. Houin, A. Simon, and G. Beck: 'Relationship between structure and mechanical properties of pearlite between 0.2% and 0.8%C', *Transactions of the Iron and Steel Institute of Japan*, 1981, **21**, 726–731.

33. K. Nakase, and I. M. Bernstein: 'The effect of alloying elements and microstructure on the strength and fracture resistance of pearlitic steel', *Metallurgical Transactions A*, 1988, **19**, 2819–2829.

34. D. J. Alexander, and I. M. Bernstein: 'Cleavage fracture in pearlitic eutectoid steel', *Metallurgical Transactions A*, 1989, **20**, 2321–2335.

35. C. M. Bae, C. S. Lee, and W. J. Nam: 'Effect of carbon content on mechanical properties of fully pearlitic steels', *Materials Science and Technology*, 2002, **18**, 1317–1321.

36. J. Toribio: 'Relationship between microstructure and strength in eutectoid steels', *Materials Science & Engineering A*, 2004, **387-389**, 227–230.

37. A. M. Elwazri, P. Wanjara, and S. Yue: 'The effect of microstructural characteristics of pearlite on the mechanical properties of hypereutectoid steel', *Materials Science & Engineering A*, 2005, **404**, 91–98.

38. Y. S. Jang, M. P. Phaniraj, D. I. Kim, J. H. Shim, and M. Y. Huh: 'Effect of aluminum content on the microstructure and mechanical properties of hypereutectoid steels', *Metallurgical & Materials Transactions A*, 2010, **41**, 2078–2084.

39. S. Behera, R. K. Barik, M. B. Sk, R. Mitra, and D. Chakrabarti: 'Recipe for improving the impact toughness of high-strength pearlitic steel by controlling the cleavage cracking mechanisms', *Materials Science & Engineering A*, 2019, **764**, 138256.

40. J. A. Mohandesi, and M. Saadatmand: 'The optimization of interlamellar spacing in a nanopearlitic lead-patented hypoeutectoid steel wire', *Journal of Materials Engineering and Performance*, 2011, **20**, 1467–1473.

41. N. Tsuji, Y. Ito, Y. Saito, and Y. Minamino: 'Strength and ductility of ultrafine grained aluminium and iron produced by ARB and annealing', *Scripta Materialia*, 2002, **47**, 893–899.

42. Y. Tomota, K. Kuroki, T. Mori, and I. Tamura: 'Tensile deformation of two ductile phase alloys: flow curves of α/γ Fe-Cr-Ni alloys', *Materials Science & Engineering*, 1976, **24**, 85–94.

43. H. K. D. H. Bhadeshia, and D. V. Edmonds: 'Analysis of the mechanical properties and microstructure of a high-silicon dual phase steel', *Metal Science*, 1980, **14**, 41–49.

44. Y. Wang, Y. Tomota, T. Ohmura, W. Gong, S. Harjo, and M. Tanaka: 'Continuous and discontinuous yielding behaviors in ferrite-cementite steels', *Acta Materialia*, 2020, **196**, 565–575.

45. A. C. C. Reis, and L. Kestens: 'Cross-sectional texture gradients in interstitial free steels processed by accumulated roll bonding', *Solid State Phenomena*, 2005, **105**, 233–238.

46. A. J. E. Foreman: 'The bowing of a dislocation segment', *Philosophical Magazine*, 1967, **15**, 1011–1021.

47. J. G. Sevillano: 'On the yield and flow stress of lamellar pearlite', In: *Strength of Metals and Alloys*. Oxford, U. K.: Pergamon Press, 1979:819–824.

48. H. K. D. H. Bhadeshia: Theory of Transformations in Steels: London, U.K.: CRC Press, Taylor and Francis Group, 2021.

49. W. Fu, T. Furuhara, and T. Maki: 'Effect of Mn and Si addition on microstructure and tensile properties of cold-rolled and annealed pearlite in eutectoid Fe–C alloys', *ISIJ International*, 2004, **44**, 171–178.

50. J. Chance, and N. Ridley: 'Chromium partitioning during isothermal transformation of a eutectoid steel', *Metallurgical Transactions A*, 1981, **12A**, 1205–1213.

51. D. J. C. MacKay: 'Bayesian interpolation', *Neural Computation*, 1992, **4**, 415–447.

52. D. J. C. MacKay: 'Bayesian non-linear modelling for the energy prediction competition', *ASHRAE Transactions*, 1994, **100**, 1053–1062.

53. D. J. C. MacKay: Information Theory, Inference, and Learning Algorithms: Cambridge University Press, 2003.

54. D. J. C. MacKay: 'Probable networks and plausible predictions – a review of practical Bayesian methods for supervised neural networks', *Computation in Neural Systems*, 1995, **6**, 469–505.